Preprints of the 19th World Congress
The International Federation of Automatic Control
Cape Town, South Africa. August 24-29, 2014

Design, Modelling and Control of a Manoeuvrable Swimming Micro-Robot

H. Nourmohammadi* and J. Keighobadi**

* *Mechanical Engineering Department, University of Tabriz, Tabriz, Iran, (e-mail: hnourmohammadi@tabrizu.ac.ir)*
** *Mechanical Engineering Department, University of Tabriz, Tabriz, Iran, (e-mail: keighobadi@tabrizu.ac.ir)*

Abstract: Biomedical application of swimming microrobots such as controlled drug delivery, microsurgery and diseases monitoring have made the researches conspicuous in MEMS technology. In this paper, inspired by the flagellar motion of microorganisms (i.e. bacteria) in nature, a 3-DOF swimming microrobot is developed and analyzed. The body of the microrobot is driven by use of three prokaryotic flagella. The rotation of each flagellum in the fluid media leads to propulsion in the microrobot. At first, attention is focused on the dynamic modeling of the microrobot's motion and then, a suitable controller is designed for its tracking performance. We use resistive-force theory to derive the propulsion force generated by the flagella. Feedback linearization method is used to control the motion of the swimming microrobot for tracking performance. It is seen that, by applying three flagella, the microrobot enables to do 3-D maneuvers. The results show that the tracking performance is guaranteed by use of the designed controller and the microrobot can be controlled to do desired maneuvers and follow the desired trajectory.

Keywords: Swimming microrobot, Prokaryotic Flagella, Dynamic modeling, Tracking control.

1. INTRODUCTION

Swimming microrobots have the potential to be implanted inside the human bodies and perform some complex tasks such as accurate drug delivery, minimally invasive surgery, kidney stone removal and diseases identification (Li et al. (2009) and Nelson et al. (2010)). To acquire these aims, it is essential that, microrobots be able to perform 3D motions with appropriate controller.

The most important part of the swimming microrobots is their propulsion mechanism. The swimming microrobot's motion occurs in very low Reynolds number ($\mathrm{Re} \ll 1$) fluid flow. This is because of the small size and low velocity of microswimmer as well the hydrodynamic features of biofluid media. The very low *Re* shows that inertial forces are negligible compared to viscous forces. Considering this fact, it seems that some propulsion methodologies, originated from inertial force, are not applicable for swimming at microscale.

Inspired by the nature, several propulsion mechanisms have been proposed for swimming microrobot. Behkam et al. (2006) developed two methodologies for swimming in very low *Re* fluid flows based on prokaryotic and eukaryotic flagellar motions. Kosa et al. (2007) presented a new propulsion mechanism for microswimmer based on traveling wave in an elastic tail. Ghanbari et al. (2011) presented a novel propulsion methodology based on ciliary motion which is inspired by the protozoan paramecium.

There are other works concentrated on the control of swimming microrobots in the literature. Mahoney et al. (2011) designed a velocity control for a magnetically actuated flagellar microswimmer. Marino et al. (2012) advanced robust H_∞ technique to control the motion of an electromagnetic microswimmer with parameter uncertainties in the dynamic model of the system.

Here, attention is focused on modelling and Control of an electrically actuated swimming microrobot using helical flagella for propulsion. We concentrate on analysing 3-D dynamics of a flagellar swimming microrobot and designing appropriate controller to make it accomplish desired manoeuvres.

2. CONCEPT

Inspired by biological propulsion mechanisms, we propose a 3-DOF swimming microrobot. The propulsion mechanism in the proposed microrobot is based on prokaryotic flagellar motion. In this design, the rotary motion of flagella is supplied by microelectrical motors embedded in the body of the device. Bearing in mind the hardships corresponding to MEMS fabrication, this actuation method is more convenience compared to magnetic actuation. The schematic view of the proposed microrobot is shown in Fig. 1.

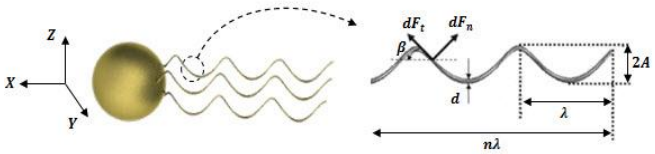

Fig. 1. Schematic view of the proposed 3-DOF flagellar swimming microrobot.

According to the viscosity of the fluid (μ) and rotational frequency of flagellum, a hydrodynamic force is created when the prokaryotic flagellum rotates in the fluid media. This force results in propulsion in the swimming microrobot. The geometrical parameters of the helical flagellum and the

normal and tangential components of the hydrodynamic force, exerted on each flagellum, were specified in Fig. 1.

This microrobot utilizes three helical flagella to generate thrust movement. When all flagella rotate counterclockwise (CCW) at the same frequency, they produce a collective propulsion force which overcomes the viscous drag of microrobot body and propels it. In this case microrobot moves along a straight line. This is so-called as run. But, as soon as one or more flagella switch to clockwise (CW) rotation and/or rotate with different frequency, microrobot undergoes an abrupt change of direction and moves randomly in two or three-dimensional paths. This case is so-called as tumble. The inputs of the system are the angular velocities of flagella and the outputs are the forward velocity and angular velocities of the microrobot body about *X*, *Y*, and *Z*-axes.

Resistive-Force Theory (RFT) is applied to derive the normal and tangential components of the viscous hydrodynamic force. Considering element *ds* along the flagellum and using RFT, the corresponding normal and tangential components (dF_n, dF_t) of the viscous force are calculated. The equations driven are shown below (Hancock. (1953)):

$$dF_i = -C_i V_i ds \qquad i = n, t \tag{1}$$

The resistive coefficients for a helical flagellum (C_n and C_t) are obtained as following (Singleton et al. (2011)):

$$\begin{aligned} C_n &= \frac{4\pi\mu}{\ln(0.18\lambda/d)+0.5} \\ C_t &= \frac{2\pi\mu}{\ln(0.18\lambda/d)} \end{aligned} \tag{2}$$

Composing the normal and tangential components of F_n and F_t, the resultant force and torque along and about of the *X*-direction for each flagellum is obtained by:

$$\begin{aligned} dF_X &= dF_t \cos\beta - dF_n \sin\beta \\ dM_X &= -A\,(dF_t \sin\beta + dF_n \cos\beta) \end{aligned} \tag{3}$$

In which β is the pitch angle of the helix and is calculated by:

$$\beta = \frac{2\pi A}{\lambda} \tag{4}$$

The normal and tangential velocities of the element *ds* can be obtained from (5):

$$\begin{aligned} V_n &= -\dot{X}\sin\beta + A\,(\omega - \dot{\theta})\cos\beta \\ V_t &= \dot{X}\cos\beta + A\,(\omega - \dot{\theta})\sin\beta \end{aligned} \tag{5}$$

Where, ω and $\dot{\theta}$ are the input angular velocity of system and resistive angular velocity constructed by M_X respectively. Furthermore, there is an additional viscous torque constituted through hydrodynamic reaction between the helical flagella and the surrounding fluid flow. The *X*-component of this torque is obtained by (Lighthill. (1967)):

$$M_S = n\lambda\pi\mu d^2\dot{\theta}\cos\beta \tag{6}$$

From the derived equations, it can be concluded that, the larger values of ω and μ leads to a greater viscous hydrodynamic force and propulsion.

3. DYNAMIC MODELING

The preceding section has described the fundamental aspects of the proposed prokaryotic flagellar microswimmer. This section concerned with the dynamic model of the 3-D motion of the proposed swimming microrobot. Microrobot's body is considered as a sphere. Three helical flagella are mounted symmetrically on the body. The angular distance between flagella is *120*º. Position of flagella and free body diagram of the swimming microrobot are shown in Fig. 2.

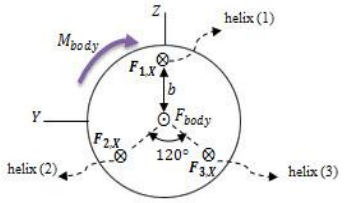

Fig. 2. Free body diagram of the 3-Dof flagellar microswimmer.

Under low *Re* fluid flow, the inertial forces can be neglected. Hence, the system of forces acted on the flagella and the body of the swimming microrobot must be in static equilibrium. The following the governing equations based on force balance along the *X*-direction and torque balance about *X*, *Y*, and *Z*-axes are set up:

$$\sum F_{X,helix} + F_{X,body} = 0 \tag{7}$$

$$\sum M_{i,helix} + M_{i,body} = 0 \qquad i = X, Y, Z \tag{8}$$

Where, F_X is the propulsion force and, M_X, M_Y and M_Z are the resultant torques constructed by the viscous forces acted on the flagella. Also, $F_{X,body}$ and $M_{i,body}$ characterize the drag force and torque, respectively. Considering Stokes flow, the drag force and torque for a sphere with the radius of a are calculated by:

$$F_{X,body} = 6\pi\mu a\dot{X} \tag{9}$$

$$M_{i,body} = 8\pi\mu a^3\Omega_i \qquad i = X, Y, Z \tag{10}$$

Where, $\dot{X}$ and Ω_i show the local linear and angular velocities of the body into the fluid flow. Substituting (1) and (5) in the (3) and integrating for $X \in [0 \;\; n\lambda]$ leads to:

$$\begin{aligned} F_{i,X} = {} & An\lambda(C_n - C_t)(\omega_i - \dot{\theta})\sin\beta - \\ & n\lambda(C_n \sin^2\beta\sec\beta + C_t\cos\beta)\dot{X} \qquad i = 1,2,3 \end{aligned} \tag{11}$$

$$\begin{aligned} M_X = {} & -A^2 n\lambda(C_n\cos\beta + C_t\sin^2\beta\sec\beta)(\omega_1 + \omega_2 + \omega_3 - 3\dot{\theta}) + \\ & An\lambda(C_n - C_t)\dot{X}\sin\beta \end{aligned} \tag{12}$$

The equilibrium equations of (7) and (8) can be rewritten as:

$$F_{1,X}+F_{2,X}+F_{3,X}-6\pi\mu a\dot{X}=0 \tag{13}$$

$$M_X+3M_S-8\pi\mu a^3\dot{\theta}=0 \tag{14}$$

$$F_{1,X}b-(F_{2,X}+F_{3,X})b/2-8\pi\mu a^3\dot{\psi}=0 \tag{15}$$

$$\sqrt{3}/2(F_{3,X}-F_{2,X})b-8\pi\mu a^3\dot{\varphi}=0 \tag{16}$$

Where the angular velocities about *X*, *Y*, and *Z*-axes are specified as $\dot{\theta}$, $\dot{\psi}$ and $\dot{\varphi}$, respectively. $F_{1,X}$, $F_{2,X}$ and $F_{3,X}$, the propulsion forces correspond to each flagellum, and M_X, the viscous torque have been defined in (11) and (12). Also the torque M_S has been determined in (6). Using (13)-(16), the following relationships can be derived for the propulsion velocity and angular velocities of the swimming microrobot.

$$\dot{X}=\frac{p_1p_5}{A^2n\lambda(p_2p_3-p_4)+p_2p_5}(\omega_1+\omega_2+\omega_3) \tag{17}$$

$$\dot{\theta}=\frac{A^2n\lambda(p_2p_3-p_4)}{A^2n\lambda(p_2p_3-p_4)+p_2p_5}(\omega_1+\omega_2+\omega_3) \tag{18}$$

$$\dot{\psi}=\frac{p_1b}{8\pi\mu a^3}(2\omega_1-\omega_2-\omega_3) \tag{19}$$

$$\dot{\varphi}=\frac{\sqrt{3}p_1b}{16\pi\mu a^3}(\omega_3-\omega_2) \tag{20}$$

And the parameters p_1 to p_5 have been defined as following:

$$\begin{aligned}
p_1&=n\lambda A(C_n-C_t)\sin\beta\\
p_2&=n\lambda(C_n\sin^2\beta\sec\beta+C_t\cos\beta)+6\pi\mu a\\
p_3&=C_n\cos\beta+C_t\sin^2\beta\sec\beta\\
p_4&=n\lambda(C_n-C_t)^2\sin^2\beta\\
p_5&=8\pi\mu a^3+3n\lambda\pi\mu d^2\cos\beta
\end{aligned} \tag{21}$$

From (17)-(20), one can conclude that, there are no rotations about *Y* or *Z*-axes when all of the three flagella rotate with the same frequencies and microrobot moves along a straight line. But any change in the frequency of each flagellum leads to two or three-dimensional motions.

4. TRACKING CONTROL

The ability of doing 3-D motion has been provided for the microrobot. But it must be noticed, this ability without applying suitable control cannot be significantly applicable. Taking into account the crucial biomedical applications of swimming microrobots, one can see the necessity of control in this work. The fundamental control strategy in this study is to make microrobot accomplish desired manoeuvre and track desired trajectory.

It should be noticed that (17) is defined in the body frame which continuously rotates when the microrobot moves along a non-straight line. Defining (*x*-*y*-*z*) as reference coordinates, the forward velocity of $\dot{X}$ is divided in three components:

$$\begin{aligned}
\dot{x}&=\dot{X}\cos\psi\cos\varphi\\
\dot{y}&=\dot{X}(\omega_1+\omega_2+\omega_3)\cos\psi\sin\varphi\\
\dot{z}&=-\dot{X}(\omega_1+\omega_2+\omega_3)\sin\psi
\end{aligned} \tag{22}$$

By this transmission, the position of swimming microrobot can be determined and controlled more easily. Choosing the desired trajectory, the magnitude of ψ_d and φ_d is determined. Then a suitable control law is designed so that ψ and φ conform to ψ_d and φ_d. As the result of this, microrobot is made to track the desired trajectory. Considering the following function as a general form of desired path,

$$\begin{cases}y_d=f_d(x_d)\\ z_d=g_d(x_d)\end{cases} \tag{23}$$

The rotation angles, corresponded to this curve (see Fig. 3) can be determined through following relations.

$$\varphi=\cos^{-1}\left(\frac{\dot{x}}{\sqrt{\dot{x}^2+\dot{y}^2}}\right)=\cos^{-1}\left(\frac{dx}{\sqrt{(dx)^2+(dy)^2}}\right) \tag{24}$$

$$\psi=\cos^{-1}\left(\frac{\sqrt{\dot{x}^2+\dot{y}^2}}{\sqrt{\dot{x}^2+\dot{y}^2+\dot{z}^2}}\right)=\cos^{-1}\left(\sqrt{\frac{(dx)^2+(dy)^2}{(dx)^2+(dy)^2+(dz)^2}}\right) \tag{25}$$

Using (24) and (25), one can determine ψ_d and φ_d for the desired trajectory. Now the control input, angular velocity of flagella, must be designed so that the rotational angles of ψ and φ track the desired values of ψ_d and φ_d respectively.

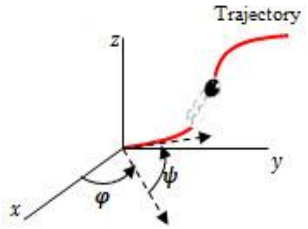

Fig. 3. Desired trajectory of the microrobot and rotational angles.

Dynamic system that must be controlled was defined beforehand by (19) and (20). Feedback linearization method (Slotine, E. (1991)) is used to control the motion of the swimming microrobot for tracking performance. In feedback linearization which is a model-based control method, inverse dynamics of system is used to design an appropriate control law. Based on this method, the control law can be defined as:

$$2\omega_1-\omega_2-\omega_3=(8\pi\mu a^3/p_1b)(\dot{\psi}_d-k_1\tilde{\psi}) \tag{26}$$

$$\omega_3-\omega_2=(16\pi\mu a^3/\sqrt{3}p_1b)(\dot{\varphi}_d-k_2\tilde{\varphi}) \tag{27}$$

Where k_1 and k_2 are positive constants and also $\tilde{\psi}$ and $\tilde{\varphi}$ are tracking errors defined by (28).

$$\tilde{\psi} = \psi - \psi_d$$
$$\tilde{\varphi} = \varphi - \varphi_d \quad (28)$$

In (26) and (27), ω_2 can be selected arbitrary and then, ω_1 and ω_3 are determined. However, the magnitude of ω_2 is important in the tracking rate. The greater value of ω_2 causes the faster tracking performance. In the prokaryotic microorganisms, flagella spin with the speed of *100 Hz* (Leifson, E. (1960)). For the stability analyzing, designed control law is substituted in the dynamics equations of system and the following closed-loop dynamics are obtained.

$$\dot{\tilde{\psi}} + k_1\tilde{\psi} = 0$$
$$\dot{\tilde{\varphi}} + k_2\tilde{\varphi} = 0 \quad (29)$$

Equations (29) are called as dynamics equations of tracking error. Choosing positive constants of k_1 and k_2, one can conclude the error dynamics is exponentially stable and over time the rotational angles ψ and φ converge to desired values of ψ_d and φ_d, respectively. Therefore, perfect tracking is satisfied and the swimming microrobot follows the desired trajectory.

5. RESULTS AND DISCUSSIONS

Some open-loop tests have been carried on using dynamic model and the trajectory of motion corresponds to each test is depicted in Figs. 4-6. It is assumed that, all flagella are made of similar steel filament and the bio fluid media in which the microrobot swims has the same hydrodynamics specifications as water. The body of microrobot is considered as a sphere with the radius of *1.5 μm*. The geometrical properties of flagella are illustrated in Table 1.

Table 1. Geometrical properties of helical flagella

Parameters	Dimensions (*μm*)
wavelength, λ	0.7
Total length, $n\lambda$	3.5
Filament diameter, d	0.02
Amplitude, A	0.25
Offset distance, b	1.0

In first test, all of the three flagella have the same frequency and the microrobot moves along a straight line (Fig. 4). In the second, when rotational frequencies of two flagella are the same and different to the frequency of third flagellum, the microrobot has a circular motion (Fig. 5), and in the third test, it has been demonstrated when all three flagella rotate with different frequencies, the swimming microrobot maneuvers in a three dimensional path (Fig. 6).

When all flagella rotate with the same frequency, three equal propulsion forces are generated in the x-direction by each flagellum. Therefore, there is no rotation about *y* or *z*-direction. But when one of the flagella has a frequency different to others, the resultant non-equal propulsion forces construct torque about *y* or *z*-axes and microrobot moves along a two and/or three-dimensional path.

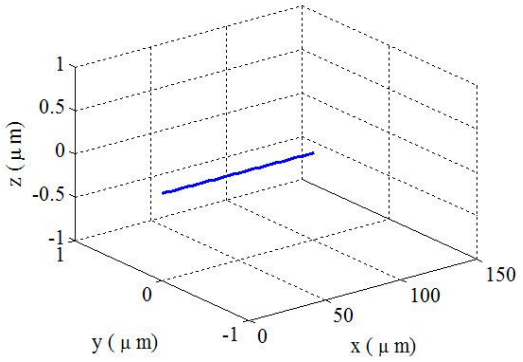

Fig. 4. Microrobot's trajectory in the first open-loop test ($\omega_1 = \omega_2 = \omega_3 = 25\ Hz$). When all of the flagella rotate with the same frequency, microrobot has a one-dimensional motion.

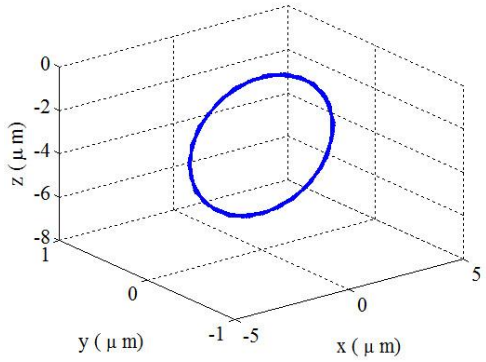

Fig. 5. Microrobot's trajectory in the second open-loop test ($\omega_1 = 25\ Hz$, $\omega_2 = \omega_3 = 15\ Hz$). When two flagella rotate with the same frequency and different to another one, microrobot has a two-dimensional motion.

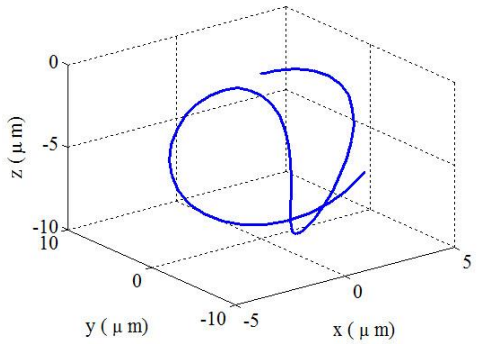

Fig. 6. Microrobot's trajectory in the third open-loop test ($\omega_1 = 25Hz$, $\omega_2 = 15Hz$, $\omega_3 = 20Hz$). When all of the flagella rotate with different frequencies, microrobot has a three-dimensional motion.

Another test is designed to investigate the control performance of the proposed swimming microrobot. In this test the desired trajectory has been defined as:

$$\begin{cases} y_d = 10^4 x_d^{\,2} \\ z_d = 10^7 x_d^{\,3} \end{cases} \quad (30)$$

Since microrobot motion happens in very low order

$(10^{-6} \sim 10^{-4})$, the large coefficients $(10^4, 10^7)$ are applied to amplify the magnitude of y_d and z_d. Using (24) and (25) the desired values of φ and ψ would be obtained. The behavior of the designed controller and trajectory tracking performance of microrobot's motion is shown in Figs. 7-10.

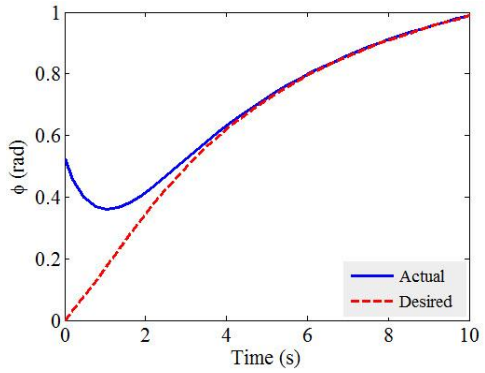

Fig. 7. Tracking of φ, simulation results of closed-loop system with tracking controller.

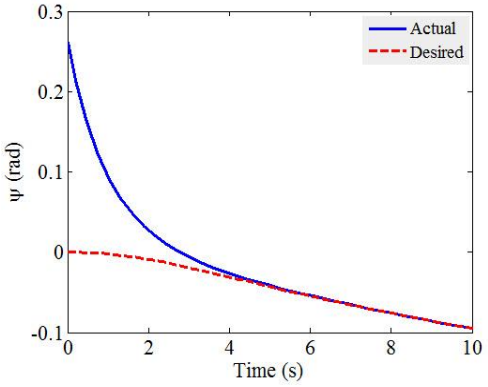

Fig. 8: tracking of ψ, simulation results of closed-loop system with tracking controller.

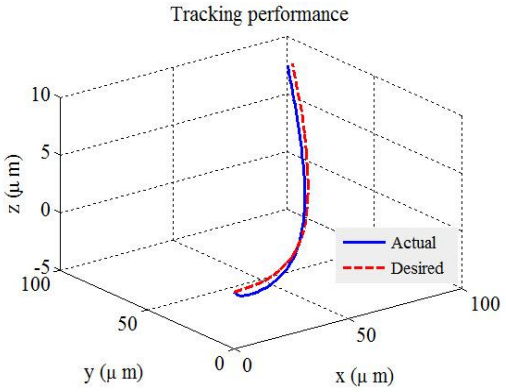

Fig. 9. Trajectory tracking performance. Microrobot follows the desired trajectory by applying the designed controller.

In this closed-loop test, the initial values of φ and ψ were defined as $\pi/6$ and $\pi/12$ respectively. It can be seen in Figs. 7 and 8 that by applying the designed controller, the rotational angles φ and ψ track the desired values. Over time, the variation rate of these angles decreases and after 5 seconds they change with a relatively less gradient. In this situation the control inputs of ω_1, ω_2 and ω_3 converge to a constant value as seen in Fig. 10.

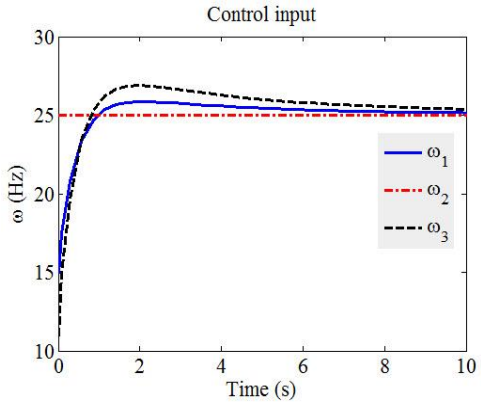

Fig. 10. Control input, required frequencies of the flagella for satisfying the tracking performance.

As stated previously, the magnitude of ω_2 is important only in the tracking rate and can be chosen arbitrary. In the simulation, the magnitude of ω_2 has been considered as 25 *Hz* and two others frequencies are determined by the designed control law. At the beginning, the rotational angles change with higher gradient and the largest control effort is required. However, the simulation results show that perfect tracking is considerably guaranteed by applying the controller and the swimming microrobot has the ability of following the desired trajectory.

6. CONCLUSIONS

Advances swimming microrobots design, analysis, and experiments have attracted significant attention particularly in medicine and biomechanics fields. Several swimming microrobots which use flagellar mechanism for propulsion have been presented in the literature. Most of the works already reported in the literature consider one and/or two dimensional motion. Here, we proposed a three degrees-of-freedom flagellar swimming microrobot. In our design, the propulsion is supplied by using multiple helical flagella i.e., prokaryotic flagella. Three helical flagella were embedded on the body of microrobot in the equal and symmetric distances. Due to the miniature sizes and low velocity of swimming microrobots, the Reynolds number corresponding to their fluid flow motion is in the very low order. So the viscous forces play more significant role in dynamic modeling compared to inertial forces. Resistive-force theory was applied to model the hydrodynamics of flagella and determine the propulsion force. Based on RFT the hydrodynamic forces are proportional to the local body velocity. All flagella are similar to each other, completely. The results of open-loop tests showed that three flagella are sufficient to cause a three-dimensional motion in the swimming microrobot. It has seen when all flagella spin with the same frequency, the microrobot swims along a straight line. When rotational frequencies of two flagella are the same and different to the frequency of third flagellum, the microrobot has a circular motion, and when all three flagella rotate with different frequencies, the swimming microrobot maneuvers in three dimensional path. Since microrobots must move freely, for instance in the human body to perform some medical duty, their position need to be specified and controlled. We used feedback

linearization method to control the microrobot's maneuvers. According to simulation results, it is observed that the swimming microrobot has the ability of doing desired maneuver and then, tracking a desired trajectory with a considerable precision.

REFERENCES

Behkam, B. and Sitti M. (2006). Design methodology for biomimetic propulsion of miniature swimming robot. *Trans ASME J Dynamic Systems, Measurement and Control*, Vol. 128, pp. 36-43.

Ghanbari, A. and Bahrami, M. (2011). A novel swimming microrobot based on artificial cilia for biomedical application. *Journal of Intelligent and Robotic Systems,* Vol. 63, pp. 399-416.

Hancock, G. (1953). The self-propulsion of microscopic organisms through liquids. *In: Proc. R Soc. London*, Ser. A, Vol. 217, pp.96-121.

Kosa, G., Shoham, M. and Zaaroor M. (2007). Propulsion method for swimming microrobots. *IEEE Transaction on Robotics*, Vol. 23, pp. 137-150.

Leifson, E. (1960). *Atlas of bacterial flagellation*, New York, Academic press.

Li, H., Tan, J. and Zhang, M. (2009). Dynamics modelling and analysis of a swimming microrobot for controlled drug delivery. *IEEE Transactions on Automation Science and Engineering,* Vol. 6, pp. 220-227.

Lighthill, J. (1976). Flagellar hydrodynamics. *SIAM Review*, Vol. 18, pp. 161-230.

Mahoney, A., Sarrazin, J.C., Bamberg, E. and Abbott J.J. (2011). Velocity control with gravity compensation for magnetic helical microswimmers. *Journal of Advanced Robotics,* Vol. 25, pp. 1007–1028.

Marino, H., Bergeles, C. and Nelson. B.J. (2012). Robust H∞ control for electromagnetic steering of microrobots, *IEEE International Conference* on *Robotic and Automation (ICRA).*

Nelson, B.J., Kaliakatsos, I.K. and Abbott, J.J. (2010). Microrobots for minimally invasive medicine. *Annu Rev. Biomed. Eng.*, Vol. 12, pp. 55–85.

Singleton, J., Diller, E., Anderson, T., et al. (2011) Micro–scale propulsion using multiple flexible artificial Flagella. *International conference on Intelligent Robots and Systems*, San Francisco, pp. 1687-1692.

Slotine, E. (1991). *Applied nonlinear control*, New Jersey, 07632, Prentice Hall.